Long-range and long-term interferometric tracking by static and dynamic force-clamp optical tweezers.

A. Guiggiani[1], B. Torre[2], A. Contestabile[3], F. Benfenati[3], M. Basso[1], M. Vassalli[4,*], and F. Difato[3,*]

[1] *Università di Firenze, Dipartimento di Sistemi e Informatica, Florence, Italy*
[2] *Italian Institute of Technology (IIT), Dept. of Nanophysics, Genoa, Italy*
[3] *Italian Institute of Technology (IIT), Dept. of Neuroscience and Brain Technologies, Genoa, Italy*
[4] *National Research Council of Italy, Institute of biophysics, Genoa, Italy*
** massimo.vassalli@cnr.it and francesco.difato@iit.it*

Abstract: Optical tweezers are recognized single-molecule technique to resolve forces and motion on the molecular scale. Complex biological phenomena, such as cell differentiation and locomotion, require long range tracking capabilities with nanometer resolution over an extended period, to resolve molecular processes on the cellular scale. Here we introduce a real-time control of the microscope stage position to perform long-term tracking, with sub-millisecond resolution, of a bead attached to a neuron, preserving sub-nanometer sensitivity on a spatial range of centimeters, seven orders of magnitude larger. Moreover, the suitability of the system is tested by time-modulating the force-clamp condition to study the role of statically and dynamically applied forces in neuronal differentiation.

OCIS codes: (350.4855) Optical tweezers or optical manipulation; (120.4880) Optomechanics; (120.3180) Interferometry; (170.1530) Cell analysis ; (170.1420) Biology.

References and links

1. F. Huber and J. Käs, "Self-regulative organization of the cytoskeleton," Cytoskeleton (Hoboken) **68**(5), 259–265 (2011).
2. S. Siechen, S. Yang, A. Chiba, and T. Saif, "Mechanical tension contributes to clustering of neurotransmitter vesicles at presynaptic terminals," Proc. Natl. Acad. Sci. U.S.A. **106**(31), 12611–12616 (2009).
3. D. E. Ingber, "From cellular mechanotransduction to biologically inspired engineering: 2009 Pritzker Award Lecture, BMES Annual Meeting October 10, 2009," Ann. Biomed. Eng. **38**(3), 1148–1161 (2010).
4. T. Mammoto and D. E. Ingber, "Mechanical control of tissue and organ development," Development **137**(9), 1407–1420 (2010).
5. P. Bianco, A. Nagy, A. Kengyel, D. Szatmári, Z. Mártonfalvi, T. Huber, and M. S. Kellermayer, "Interaction forces between F-actin and titin PEVK domain measured with optical tweezers," Biophys. J. **93**(6), 2102–2109 (2007).
6. S. M. Kalisch, L. Laan, and M. Dogterom, "Force generation by dynamic microtubules in vitro," Methods Mol. Biol. **777**, 147–165 (2011).
7. C. Veigel and C. F. Schmidt, "Moving into the cell: single-molecule studies of molecular motors in complex environments," Nat. Rev. Mol. Cell Biol. **12**(3), 163–176 (2011).
8. D. Cojoc, F. Difato, E. Ferrari, R. B. Shahapure, J. Laishram, M. Righi, E. M. Di Fabrizio, and V. Torre, "Properties of the force exerted by filopodia and lamellipodia and the involvement of cytoskeletal components," PLoS ONE **2**(10), e1072–e1078 (2007).
9. C. O. Mejean, A. W. Schaefer, E. A. Millman, P. Forscher, and E. R. Dufresne, "Multiplexed force measurements on live cells with holographic optical tweezers," Opt. Express **17**(8), 6209–6217 (2009).
10. A. G. Banerjee, S. Chowdhury, W. Losert, and S. K. Gupta, "Survey on indirect optical manipulation of cells, nucleic acids, and motor proteins," J. Biomed. Opt. **16**(5), 051302 (2011).
11. A. Rohrbach, C. Tischer, D. Neumayer, E. L. Florin, and E. Stelzer, "Trapping and tracking a local probe with a photonic force microscope," Rev. Sci. Instrum. **75**(6), 2197–2210 (2004).
12. H. Zhang and K. K. Liu, "Optical tweezers for single cells," J. R. Soc. Interface **5**(24), 671–690 (2008).
13. E. J. Peterman, F. Gittes, and C. F. Schmidt, "Laser-induced heating in optical traps," Biophys. J. **84**(2), 1308–1316 (2003).

#152555 - $15.00 USD Received 8 Aug 2011; revised 10 Sep 2011; accepted 10 Sep 2011; published 24 Oct 2011

14. F. Difato, E. Ferrari, R. Shahapure, V. Torre, and D. Cojoc, "Optical tweezers microscopy: piconewton forces in cell and molecular biology," in *Nanoscopy and Multidimensional Optical Fluorescence Microscopy,* A. Diaspro, ed. (Taylor & Francis, 2010).
15. K. C. Neuman and S. M. Block, "Optical trapping," Rev. Sci. Instrum. **75**(9), 2787–2809 (2004).
16. M. E. Janson and M. Dogterom, "Scaling of microtubule force-velocity curves obtained at different tubulin concentrations," Phys. Rev. Lett. **92**(24), 248101 (2004).
17. D. J. Carnegie, D. J. Stevenson, M. Mazilu, F. Gunn-Moore, and K. Dholakia, "Guided neuronal growth using optical line traps," Opt. Express **16**(14), 10507–10517 (2008).
18. D. McGloin, V. Garcés-Chávez, and K. Dholakia, "Interfering Bessel beams for optical micromanipulation," Opt. Lett. **28**(8), 657–659 (2003).
19. P. Kraikivski, B. Pouligny, and R. Dimova, "Implementing both short- and long-working-distance optical trappings into a commercial microscope," Rev. Sci. Instrum. **77**(11), 113703 (2006).
20. T. Cižmár, V. Kollárová, X. Tsampoula, F. Gunn-Moore, W. Sibbett, Z. Bouchal, and K. Dholakia, "Generation of multiple Bessel beams for a biophotonics workstation," Opt. Express **16**(18), 14024–14035 (2008).
21. R. Dasgupta, R. S. Verma, S. Ahlawat, D. Chaturvedi, and P. K. Gupta, "Long-distance axial trapping with Laguerre-Gaussian beams," Appl. Opt. **50**(10), 1469–1476 (2011).
22. R. Nambiar, A. Gajraj, and J. C. Meiners, "All-optical constant-force laser tweezers," Biophys. J. **87**(3), 1972–1980 (2004).
23. R. Bowman, G. Gibson, and M. Padgett, "Particle tracking stereomicroscopy in optical tweezers: control of trap shape," Opt. Express **18**(11), 11785–11790 (2010).
24. T. Aggarwal and M. Salapaka, "Real-time nonlinear correction of back-focal-plane detection in optical tweezers," Rev. Sci. Instrum. **81**(12), 123105 (2010).
25. S. Perrone, G. Volpe, and D. Petrov, "10-fold detection range increase in quadrant-photodiode position sensing for photonic force microscope," Rev. Sci. Instrum. **79**(10), 106101 (2008).
26. M. Capitanio, R. Cicchi, and F. S. Pavone, "Continuous and time-shared multiple optical tweezers for the study of single motor proteins," Opt. Lasers Eng. **45**(4), 450–457 (2007).
27. D. Preece, R. Bowman, A. Linnenberger, G. Gibson, S. Serati, and M. Padgett, "Increasing trap stiffness with position clamping in holographic optical tweezers," Opt. Express **17**(25), 22718–22725 (2009).
28. A. E. Wallin, H. Ojala, E. Haeggstrom, and R. Tuma, "Stiffer optical tweezers through real-time feedback control," Appl. Phys. Lett. **92**(22), 224104 (2008).
29. A. van der Horst and N. R. Forde, "Calibration of dynamic holographic optical tweezers for force measurements on biomaterials," Opt. Express **16**(25), 20987–21003 (2008).
30. V. Soni, F. M. Hameed, T. Roopa, and G.V. Shivashankar, "Development of an optical tweezer combined with micromanipulation for DNA and protein nanobioscience," Rev. Sci. Instrum. **83**, 1464–1470 (2002).
31. H. T. Ghashghaei, C. Lai, and E. S. Anton, "Neuronal migration in the adult brain: are we there yet?" Nat. Rev. Neurosci. **8**(2), 141–151 (2007).
32. S. H. Parekh, O. Chaudhuri, J. A. Theriot, and D. A. Fletcher, "Loading history determines the velocity of actin-network growth," Nat. Cell Biol. **7**(12), 1219–1223 (2005).
33. A. Mogilner, "On the edge: modeling protrusion," Curr. Opin. Cell Biol. **18**(1), 32–39 (2006).
34. R. Shahapure, F. Difato, A. Laio, G. Bisson, E. Ercolini, L. Amin, E. Ferrari, and V. Torre, "Force generation in lamellipodia is a probabilistic process with fast growth and retraction events," Biophys. J. **98**(6), 979–988 (2010).
35. F. Difato, M. Dal Maschio, E. Marconi, G. Ronzitti, A. Maccione, T. Fellin, L. Berdondini, E. Chieregatti, F. Benfenati, and A. Blau, "Combined optical tweezers and laser dissector for controlled ablation of functional connections in neural networks," J. Biomed. Opt. **16**(5), 051306 (2011).
36. F. Difato, Schibalsky L., F. Benfenati, and A. Blau, "Integration of optical manipulation and electrophysiological tools to modulate and record activity in neural networks," Int. J. Optomechatronics (to be pubblished).
37. L. Dozio and P. Mantegazza, "Real time distributed control systems using RTAI," in *Proceedings of IEEE Conference on Object-Oriented Real-Time Distributed Computing Symp.* (IEEE, 2003), pp. 11–18.
38. D. Materassi, P. Baschieri, B. Tiribilli, G. Zuccheri, and B. Samorì, "An open source/real-time atomic force microscope architecture to perform customizable force spectroscopy experiments," Rev. Sci. Instrum. **80**(8), 084301 (2009).
39. Y. C. Wenas and M. D. Hoogerland, "A versatile all-optical Bose-Einstein condensates apparatus," Rev. Sci. Instrum. **79**(5), 053101 (2008).
40. M. Basso, R. Bucher, M. Romagnoli, and M. Vassalli, "Real-Time Control with Linux: A Web Services Approach," in *Proceedings of IEEE Conference on Decision and Control, and the European Control Conference* (IEEE, 2005), pp. 2733–2738.
41. H. Babu, G. Cheung, H. Kettenmann, T. D. Palmer, and G. Kempermann, "Enriched monolayer precursor cell cultures from micro-dissected adult mouse dentate gyrus yield functional granule cell-like neurons," PLoS ONE **2**(4), e388 (2007).
42. P. C. Seitz, E. H. Stelzer, and A. Rohrbach, "Interferometric tracking of optically trapped probes behind structured surfaces: A phase correction method," Appl. Opt. **45**(28), 7309–7315 (2006).
43. M. O'Toole and K. E. Miller, "The role of stretching in slow axonal transport," Biophys. J. **100**(2), 351–360 (2011).

#152555 - $15.00 USD Received 8 Aug 2011; revised 10 Sep 2011; accepted 10 Sep 2011; published 24 Oct 2011

44. V. Vogel and M. P. Sheetz, "Cell fate regulation by coupling mechanical cycles to biochemical signaling pathways," Curr. Opin. Cell Biol. **21**(1), 38–46 (2009).
45. G. Giannone, B. J. Dubin-Thaler, O. Rossier, Y. Cai, O. Chaga, G. Jiang, W. Beaver, H. G. Döbereiner, Y. Freund, G. Borisy, and M. P. Sheetz, "Lamellipodial actin mechanically links myosin activity with adhesion-site formation," Cell **128**(3), 561–575 (2007).
46. K. E. Kubow, E. Klotzsch, M. L. Smith, D. Gourdon, W. C. Little, and V. Vogel, "Crosslinking of cell-derived 3D scaffolds up-regulates the stretching and unfolding of new extracellular matrix assembled by reseeded cells," Integr. Biol. **1**(11-12), 635–648 (2009).
47. O. M. Rossier, N. Gauthier, N. Biais, W. Vonnegut, M. A. Fardin, P. Avigan, E. R. Heller, A. Mathur, S. Ghassemi, M. S. Koeckert, J. C. Hone, and M. P. Sheetz, "Force generated by actomyosin contraction builds bridges between adhesive contacts," EMBO J. **29**(6), 1055–1068 (2010).
48. J. Fouchard, D. Mitrossilis, and A. Asnacios, "Acto-myosin based response to stiffness and rigidity sensing," Cell Adhes. Migr. **5**(1), 16–19 (2011).
49. J. Rajagopalan, A. Tofangchi, and M. T. A. Saif, "*Drosophila* neurons actively regulate axonal tension in vivo," Biophys. J. **99**(10), 3208–3215 (2010).
50. M. Allioux-Guérin, D. Icard-Arcizet, C. Durieux, S. Hénon, F. Gallet, J. C. Mevel, M. J. Masse, M. Tramier, and M. Coppey-Moisan, "Spatiotemporal analysis of cell response to a rigidity gradient: a quantitative study using multiple optical tweezers," Biophys. J. **96**(1), 238–247 (2009).
51. D. Mitrossilis, J. Fouchard, D. Pereira, F. Postic, A. Richert, M. Saint-Jean, and A. Asnacios, "Real-time single-cell response to stiffness," Proc. Natl. Acad. Sci. U.S.A. **107**(38), 16518–16523 (2010).

1. Introduction

How molecular motors coordinate and synchronize in cells [1] to produce complex functions such as cell locomotion, cell-cell connections [2], or mechanical transduction [3] and how mechanical tension plays a role in cell development, are becoming an intriguing research field [4]. Several studies applied optical tweezers to characterize molecular motor mechanics under load in *vitro* [5]. However, understanding how such motors perform in the cellular context is hampered by technical challenges that are still to be solved [6]. First of all, trapping and tracking particles inside a cell are complex tasks because the cytoplasm is a highly viscous and scattering medium which affects the manipulation of the particle and makes the calibration of the optical system difficult [7]. Therefore, optical tweezers studies at cellular level were conducted by manipulation of external functionalized probes close to the cell [8,9] or attached to the plasma membrane [10]. In these works, limiting factors for long time investigations were represented by local heating inducing cellular photo-damage as well as the narrow linear range of the interferometric tracking system [11]. While the photo-damage limits the viability of the cells and consequently the time window of observation, the linear range of the detector constrains the force measurement on about 250 nm around the center of the trap [12]. Increasing the stiffness of the trap could help confining the cellular fluctuations within this linear range, but it results in a lower force sensitivity and shorter viability of the cells due to increased laser power at the sample [13,14]. Although photo-damage at quite high laser power can be reduced by properly choosing the laser wavelength, as previously reported in several studies, commercial systems do not always have the high beam quality required for efficient trapping, and therefore a compromise between spectral properties and laser efficiency has to be traded while choosing the laser system [15]. An alternative and promising strategy is to extend the spatial range of measurement allowing for a lower optical stiffness (i.e. laser power at the sample), which results in a minimization of the photo-damage and in an increase of the useful timeframe for the experiment. To achieve this goal, researchers adopted several approaches relying on laser beam shaping, experimental characterization of the unique range of the detector response, or real time control of the optical trap position.

Laser beam shaping by intensity [16] or phase modulation [17,18] have been adopted to create an extended one-dimensional optical potential, Bessel beam optical tweezers, or long working distance optical trapping [19]. With such methods, the trapping volume is enlarged, allowing for asymmetric particle trapping and alignment, as well as particle laser guiding over a range of about 1 mm [20,21]. In order to increase the linear range of detection trapping stiffness in the two directions orthogonal to the elongated dimension of the laser beam can be considered constant, to perform force spectroscopy along a laser line focus of few

#152555 - $15.00 USD Received 8 Aug 2011; revised 10 Sep 2011; accepted 10 Sep 2011; published 24 Oct 2011

micrometers [22]. Another strategy actuates the shaping of the beam to concentrate the major of the laser light at the extremes of the objective back aperture, thus creating a more efficient axial trapping. However, such method produces a more efficient confinement of the measured biological fluctuations in the focus trap, but does not increase the linear range of the detection system [23].

Other researchers proposed to experimentally characterize the detector properties to expand the area where conduct force spectroscopy measurements. Polynomial fitting of the measured unique range of the detector response allows to apply these measurements out of the linear portion of detector response [24]. Moreover, considering the cross talk between the four quadrant signals allows to further enlarge the unique range of the detector, reaching more than one micrometer [25].

However, such increased range is not sufficient for many applications on single molecular motors and therefore, a real-time control of the optical trap position becomes mandatory. Two main approaches are illustrated in literature. One is based on the introduction of acousto-optic devices, which deflect the laser beam with a bandwidth of few kHz [26]. A second strategy is based on the use of a spatial light modulator, which has a refresh bandwidth of a few hundreds Hz [27]. These methods implement feedback control with relatively large bandwidth, while allowing for an increase of the trap stiffness [28]. However they lead to changes in the optical path of the system and therefore, they present the drawback that the optical stiffness of the optical setup remains constant for small displacement of laser focus in the sample plane (few tens of micrometers) [29]. A distinct approach is based on real-time positioning of the microscope stage position with respect to a fixed laser beam focus, thus keeping the optical properties of the system unchanged. This method introduces a feedback control of the stage position with a typical bandwidth up to 100 Hz [30], over a spatial range limited only by the coarse motion of the piezoelectric stage (usually in the order of few hundreds of micrometers).

Given that cells and more specifically neurons migrate or extrude neuritis over distances of several millimeters during their development [31]. While molecular motors move with a speed below 1 μm/sec and with kHz bandwidth [32,33], cell motility reaches rates of tens of micrometers per minute with bandwidths of a few tens of Hz [34]. Therefore, in order to detect molecular dynamics during cell motility, we combine a nanometric piezoelectric stage with a micrometric motorized positioning system. This approach will go beyond the compromise between sensitivity and working range, allowing for nanometer and sub-millisecond resolution over millimeter spatial range, covering the cellular scale of motion.

2. Material and methods

2.1. Optical setup

The entire optical system has been described in detail elsewhere [35]. Briefly, the trapping source was an ytterbium continuous wave (CW) fiber laser operating at 1064 nm (IPG Laser GmbH). The phase of the IR laser beam was modulated trough a spatial light modulator (SLM) (LCOS-SLM, model X10468-07 – Hamamatsu). The interferometer for force spectroscopy measurements was based on a four-quadrant photodiode (QPD, S5980 with C5460SPL 6041 board – Hamamatsu) and a photodiode PD2 (PDA100A-EC - Thorlabs). Electrical signals coming from the four quadrants of the QPD and PD2 are amplified 100-fold (2 amplifier boards: MULTIBOARD, Sglux) and then digitized independently by an analog-to-digital (A/D) data acquisition converter (NI PCI-6229, M Series DAQ - National Instruments).

The holographic tweezers module was integrated on a modified upright microscope (BX51 – Olympus) equipped with a 60X, 0.9 NA water dipping objective.

The stage of the microscope was composed of a 3-axis linear DC motor micro-positioning system (M-126.CG1 – Physics-Instruments) carrying a separate 3-axis piezoelectric nano-

#152555 - $15.00 USD Received 8 Aug 2011; revised 10 Sep 2011; accepted 10 Sep 2011; published 24 Oct 2011

positioning stage (P-733.3DD – Physics-Instruments) to combine coarse movement of the sample with the sub-nanometer resolution of the piezoelectric stage.

On the micro-positioning system a nano-manipulator (MM3-LS- Kleindiek nanotechnik) was installed.

2.2. Microscope sample chamber

Cells under the microscope were kept at 37 ^{0}C by a Peltier device (QE1 resistive heating with TC-344B dual channel heater controller -Warner Instruments). pH and humidity were controlled by aerating a custom-designed polydimethylsiloxane PDMS sleeve, which integrated the objective for optical access, with humidified carbogen (95% O_2, 5% CO_2). Cells were maintained 24 h under the microscope with no significant variation in pH and with only a small increase in osmolality of the medium due to evaporation (t = 0:4 ml, osmolality: 230 mOsmol/kg; t = 24 h, 3 ml, osmolality: 300 mOsmol/kg) [36].

2.3. Real-Time control Software

Real-time control is needed to maintain the bead within linear trapping region (distance from trapping center less than 450 nm). The goal was to generate a pilot signal for the piezoelectric actuators starting from the interferometric measurement of the bead position relative to the trap given by the photodiodes. Such control was built on a Linux *Real Time Application Interface* (RTAI) machine [37]. RTAI is a project that allows Linux machines to perform real-time signal acquisition and conditioning, that has been successfully applied to the driving of scientific experiments [38, 39]. It is based on a modified Linux kernel that allows for the execution of tasks with strict temporal constraints, called real-time targets. In addition, the RTAI suite provides a simple target generation tool-chain based on visual software like the open-source project *Scicoslab* [37]. Interface with data acquisition hardware is made through *Comedi*, a set of libraries and drivers for real-time systems, compatible with a wide range of acquisition boards. A core functionality of an RTAI-based machine is given by RTAI-XML project [40], which adds the possibility for the real-time target to communicate with a remote client over TCP/IP. This allowed for the separation of *Human Machine Interface* (HMI) components, like signal visualization and parameter editing, from the actual control machine. A machine based on RTAI is highly flexible and controllable algorithm design and showed high performances, with sampling rates in the range of kHz. It is also cheap to build, since all that is needed is a commercial PC paired with a data acquisition board.

The real-time control target used in the experiments, running on a RTAI machine, was structured with nine analog channels, which were acquired and sampled at 2 kHz rate (three of these channels were used for interferometric photodiodes measurements of bead displacement along the three axes. Another three channels were employed for capacitive sensors measurements of piezoelectric stage, and the last three were devoted to external, dynamic references coming from wave generators). The system was equipped with two control loops, synergically acting to maintain the system at the right position, depending on the selected working mode (position or force clamp, static or dynamic). In particular, an internal loop acts on a fast response – short dynamics piezoelectric stage, to keep the bead at a selected distance from the trap center (or, in other words, to keep the force constant). Moreover, a second external loop controls the position of a slower motorized stage, aimed at maintaining the region spanned by the piezo-actuator in the central portion of the available stroke. Both these feedbacks were of proportional/integral type, with integral anti-windup compensation. Four signals were sent as output to the D/A interface: three as control signal, one for each piezoelectric stage axis; the fourth acted as a trigger for the camera to sync video acquisition with data logging. Thanks to RTAI-XML implementation, real-time target streams over TCP/IP stage positions and photodiodes measurements, and it can be accessed to change the control parameters. A second machine, through a custom user interface, allowed visualization and saving of the measurements, and provided a graphical front-end for control

#152555 - $15.00 USD Received 8 Aug 2011; revised 10 Sep 2011; accepted 10 Sep 2011; published 24 Oct 2011

parameters editing (e.g. proportional and integral gains). Alongside with data and parameter handling, the interface managed automatic micro-stage recoveries to extend piezo-stage range.

2.4. Bead coating

Silica beads (Ø 4 μm, COOH coated – Bangs Laboratories) were coated with poly-D-lysine following the procedure described in the PolyLink Protein Coupling Kit (Polysciences).

2.4. Cell cultures

Primary cultures were obtained from brain tissue of Sprague Dawley rats at embryonic day 18 (E18). Embryos were removed and dissected under sterile conditions. Cortices and hippocampi were dissociated by enzymatic digestion in trypsin (0.125% for 20 min at 37 °C) and then triturated with a fire-polished Pasteur pipette. Neurons were plated at a concentration of $0.25\text{-}1\cdot10^5$ cells/ml on the active area of the microelectrode arrays (MEAs) or on 35mm-diameter Petri dishes with cover glass at the bottom (P35G-0-14-C –MaTek Corporation). Substrates were previously coated with poly-D-lysine (100 μg/ml) and laminin (5 μg/ml) to support cell adhesion and differentiation. One hour after seeding, the MEA reservoir was filled with 1 ml of serum-free medium (Neurobasal with 2% B27 supplement, 1% Glutamax and 1% penicillin/streptomycin, all purchased from Invitrogen). Cells were kept in a standard humidified CO_2 incubator (5% CO_2, 92% rh, 37°C).

Adult dentate neural precursor cells (ADNPCs) were prepared from the dentate gyrus of adult (6-8 weeks) mice as previously described [41] and maintained as monolayer cultures. Cells were cultured in Neurobasal medium containing 2% B27, 2mM Glutamax and 1% Penicillin-Streptomycin solution (all from Invitrogen) with 20 ng/ml human Fibroblast Growth Factor-2 (FGF2) and 20 ng/ml human Epidermal Growth Factor (EGF) (both from Pepro-Tech). Cells were passaged at 70-80% confluence by detaching with Accutase (PAA Laboratories) and plating at 10^4 cells/cm^2 on plastic dishes coated with 10 μg/mL poly-D-Lysine (Sigma) and 5μg/mL Laminin (Roche). For experiments cells were plated on poly-D-Lysine/Laminin coated Matek dishes.

Cell viability was evaluated after exposing cells to a power of 10 mW of the trapping laser (1064 nm wavelength), for about 40 minutes. Then the cell impermeable fluorescent dye Propidium Iodine (5 μg/ml concentration. Sigma) was added to the dish. Propidium Iodine can only enter dead cells were membrane integrity is compromised. After 5 minutes, to allow dye diffusion, the exclusion of the dye from the nucleus of irradiated cell was verified by acquiring a fluorescent image.

3. Results

3.1 Testing and calibrating the real-time feedback control

In order to perform interferometric tracking over a spatial range of several millimetres, we combined a piezoelectric stage with a micro positioning system. The piezoelectric stage (Pstage) was controlled in real-time by a feedback loop with the signal output of the QPD to follow the trapped probe, maintaining it in the centre of the trapping potential, while the micro stage (Mstage) monitored the absolute position of the Pstage (Fig. 1a). When the Pstage reaches a threshold position (see conditions in Fig. 1a), the Mstage moves in the opposite direction, inducing a re-positioning of the Pstage to maintain the force set-point.

We varied the proportional (P) and integral (I) constants (in arbitrary units) to test the capability of the real-time control to maintain the trapped probe in the potential well of the laser. In Fig. 1b, we show the displacement of a bead, stuck to the cover glass and centred in the optical trap, in response to a step motion of 400 nm actuated at a speed of 10 μm/sec.

Starting from a P value of 0.2 up to a maximum value of 10, we showed that the displacement of the bead decreased, reaching a minimum of 157 nm (the volt-nanometres

#152555 - $15.00 USD Received 8 Aug 2011; revised 10 Sep 2011; accepted 10 Sep 2011; published 24 Oct 2011

linear range, with a 4 μm Ø bead, was ± 450 nm in plane, and ± 1.8 μm in the axial direction). With a P value of 25, the control loop overcomes the stability region and the noise in the QPD signal became amplified. We therefore selected P values below such a threshold. In Fig. 1c, we tested the feedback performance for increasing values of I, in response to the same step motion as in Fig. 1b. We show that for I = 120, the time constant of the feedback reached a value of 0.08 seconds. Then, we set the speed of Mstage during the recovery motion to 0.3 μm/sec because, as it is shown in Fig. 1d, such value produced a systematic displacement of the bead, followed by the Pstage, smaller than 50 nm. Moreover, considering that the force-nanometres linear range, with a 4 μm Ø bead, was ± 250 nm in plane, and ± 500 nm in the axial direction, we ensured to work in the region of the optical trap potential where the stiffness of the system was constant.

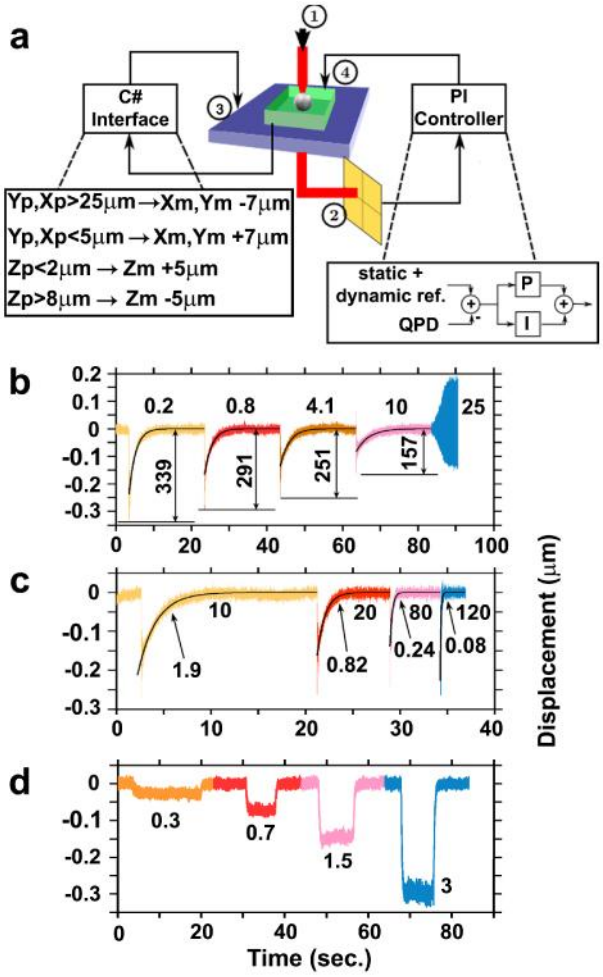

Fig. 1. System architecture and calibration. (a) Overview of the control architecture, with real-time feedback PI control of the Pstage, and automatic recoveries of the Mstage. Numbers in the black circles indicate the essential components fo the systems: (1) Optical trapping laser, (2) QPD based detection system, (3) Mstage, (4) Pstage. (b) Evaluation of feedback control behavior in response to step motion of 400 nm, actuated with a velocity of 10 μm/sec, for increasing proportional gains P. (c) Evaluation of feedback control behavior in response to step motion of 400 nm, actuated with a velocity of 10 μm/sec, for increasing integral gains I. (d) Constant tracking errors while following bead movements at various recovery velocities of the Mstage.

#152555 - $15.00 USD Received 8 Aug 2011; revised 10 Sep 2011; accepted 10 Sep 2011; published 24 Oct 2011

After calibration of the entire microscope real time control, we tested the system with a bead attached to the tip of a glass pipette (see Fig. 2b, upper panel) moved by a micromanipulator, so as to emulate the bead displacement produced by a cell. In Fig. 2a, we report the recorded traces of the Mstage, the Pstage, and the QPD signal converted in micrometers. In the central panel, the horizontal lines mark the reference point at which the Mstage started the re-positioning motion, and the coloured boxes sign the duration of the Mstage actuation. In the lower panel, the QPD traces report the bead displacement with respect to the centre position of the trap during the Mstage recovery. The bead was shifted about 100 nm, and therefore it was still in the linear range of the interferometric detector. To obtain the overall motion of the tracked bead, it was necessary to sum the QPD and Pstage traces and subtract the Mstage recovery motion (Fig. 2b). In Fig. 2c, an inset of the overall trace in Fig. 2b is illustrated. On the left the QPD traces plotted show how after each step of the manipulator, the Pstage re-positions the bead in the centre of the trap, while on the right the calculated overall motion of the bead is presented, clearly resolving the stepping motion actuated by the manipulator.

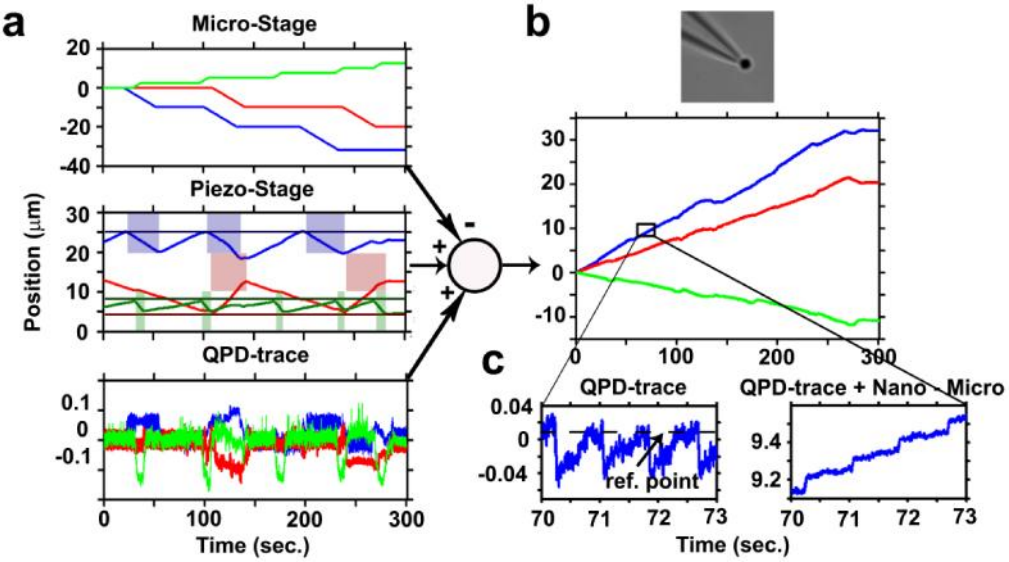

Fig. 2. A bead manipulated by a micropipette to test the tracking system performance. (a) Traces of the positions on three axes of Mstage and Pstage, and corresponding photodiodes traces. Traces of the x, y, z coordinates of the tracked bead (in blue, red and green respectively). Colored boxes show recovery phases. (b) Total movement of the bead obtained by subtracting Mstage positions to the sum of Pstage positions and QPD traces. In the upper panel, a snapshot of the bead attached to the micropipette. (c) Inset of the bead displacement from the centre of the trap, on the left (QPD trace only). On the right, bead absolute displacement with micropipette step movements and thermal noise clearly noticeable (on the right).

3.2 Living cell interferometric tracking

We applied the developed system to track the growth cone motility of differentiating rat hippocampal neurons during the first days in *vitro* (DIV). In Fig. 3a, we show a poly-D-lysine coated bead (the same type of coating used on the culture substrate) attached to the growth cone of rat hippocampal neuron (6 DIV). The Fig. 3b, illustrates the morphology of the growth cone during formation of a contact with a neurite. The growth cone turned toward the neurite on the right side, and created a first thin connection at four minutes. At 15 minutes, other filopodia extruding from the growth cone attached to the neurite, and later fused together into a thicker connection moving along the neuronal process.

#152555 - $15.00 USD Received 8 Aug 2011; revised 10 Sep 2011; accepted 10 Sep 2011; published 24 Oct 2011

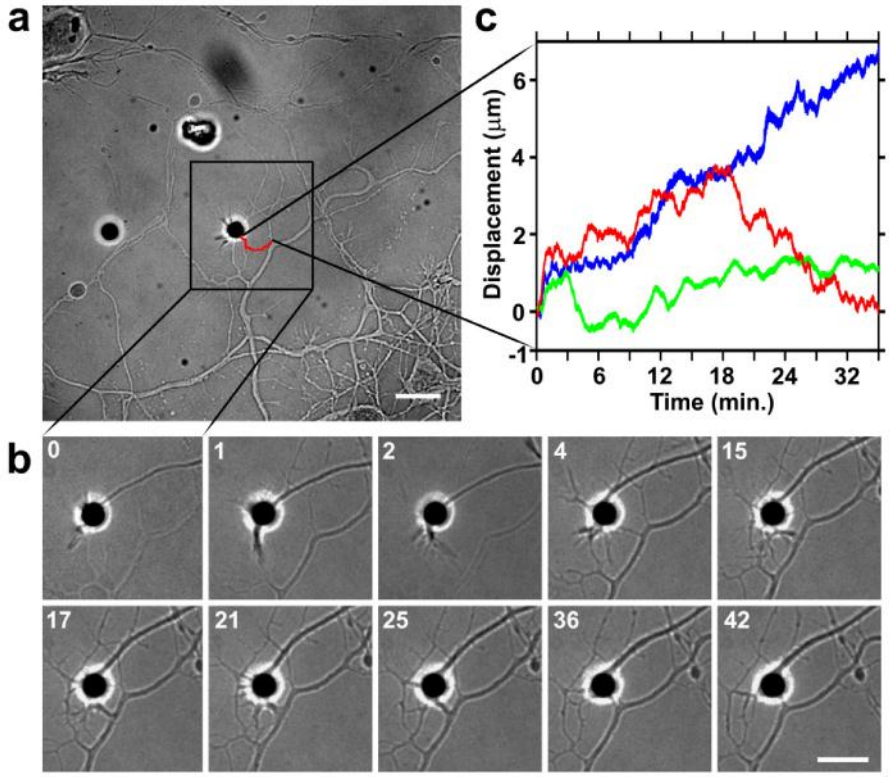

Fig. 3. A growth cone connecting to a neurite. (a) Growth cone of differentiating rat hippocampal neuron (6 DIV) with an attached poly-D-lysine coated bead. The red line indicates the trace followed by the growth cone tracked by the attached bead. (b) Tiles of the growth cone motion during the interferometric tracking, acquired by bright-field imaging at 0.3 Hz. Numbers indicate minutes. (c) Traces of the x, y, z coordinates of the tracked bead (in blue, red and green, respectively). Axes origin is at the left upper corner of the field of view in a. Traces are sampled at 2 KHz ($k_{x,y}$ = 6.5 fN/nm, k_z = 2.3 fN/nm). Power at the sample, 5.5 mW. Bars, 8 μm.

In Fig. 3c, the x, y, z traces of the tracked bead report the dynamics of the growth cone during the formation of the new contact. Therefore, we could resolve the complex dynamic of the growth cone, composed of alternating advancing and retracting phases (traces in Fig. 3c change their slope in a cyclic way, and represent an oscillating no monotonic motion trajectory).

We performed such tracking with a 4 μm diameter bead to obtain a strong interference signal on the QPD, reducing the effect of the cell structure interfering with the laser [42]. Moreover, as a further control, we compared the QPD trace with the video-tracking of the bead as reported in Cojoc et al [8].

In Fig. 4, we show a similar experiment following the dynamics of a neuronal growth cone (6 DIV) under constant tension. In order to produce such constant force on the tip of the neurite, a constant offset voltage was summed to the QPD signal, and consequently the Pstage tracked a reference point on the bead displaced 25 and 150 nm apart from the centre of the trap, in the x and y direction respectively ($k_{x,y}$ = 4.6 fN/nm). In Fig. 4a, we show the poly-D-lysine coated bead attached to the growth cones of the rat hippocampal neuron and the direction of the force applied by the white arrow. Figure 4b illustrates how the growth cone motion seems biased from such a constant force and it reverses back.

#152555 - $15.00 USD Received 8 Aug 2011; revised 10 Sep 2011; accepted 10 Sep 2011; published 24 Oct 2011

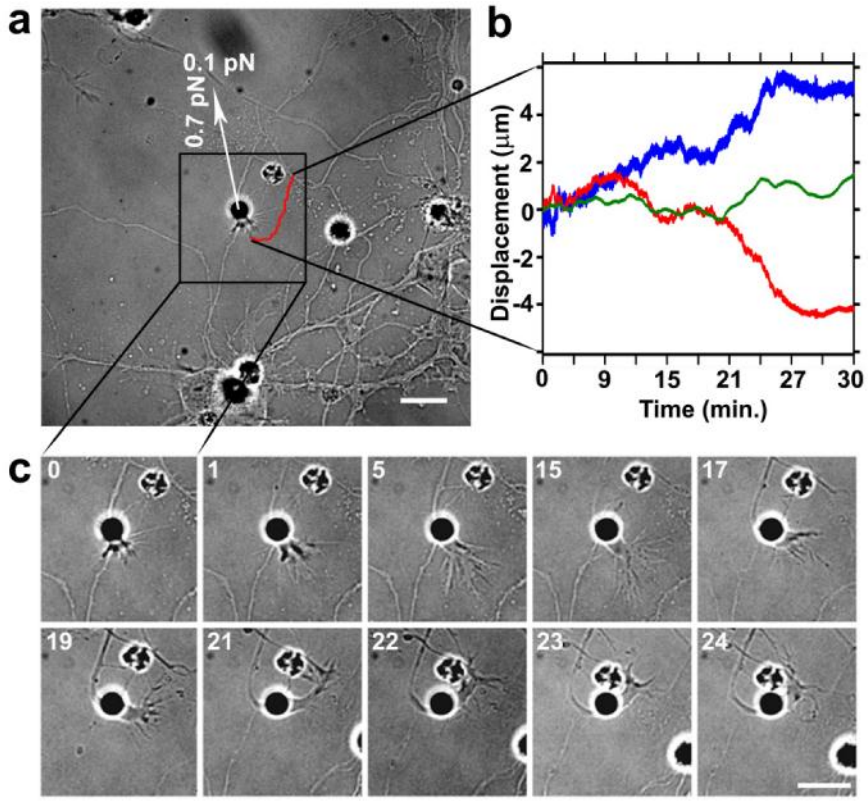

Fig. 4. A growth cone under constant tension. (a) Growth cone of differentiating rat hippocampal neuron (6 DIV) with an attached poly-D-lysine coated bead. The red line indicates the trace followed by the growth cone tracked by the attached bead. The white arrow indicates the constant force applied to the trapped bead. (b) Tiles of the growth cone motion during the interferometric tracking, acquired by bright-field imaging at 0.3 Hz. Numbers indicate minutes. (c) Traces of the x, y, z coordinates of the tracked bead (respectively in blue, red and green). Axes origin is at the left upper corner of the field of view in a. Traces are sampled at 2 KHz ($k_{x,y}$ = 4.7 fN/nm, k_z = 2.1 fN/nm). Power at the sample, 4.5 mW. Bars, 8 μm.

From the traces in Fig. 4c, it is clear that the growth cone was initially directed towards the lower right corner of the field of view in Fig. 4a. At about nine minutes, the red trace indicates how the growth cone reversed its direction. At 15 minutes, the red trace starts to grow again. If we observe the growth cone morphology at 15 minutes in Fig. 4b, this corresponds to a phase where the growth cone tried to counteract the applied force. Then, about 3 minutes later, the red trace decreased again, thus indicating that the growth cone followed the direction of the applied force. This result is surprising, considering that the applied force is smaller than 1 pN, suggesting that small tensions constantly applied for a long time can affect the growth cone motion.

In the experiment reported in Fig. 5, we attached a bead at the contact point of two growth cones extruding from the same neurite of a rat hippocampal neuron (7 DIV), and we applied a constant force in the direction indicated by the white arrow in panel 5a. Figure 5b shows the bead motion traces. The blue shadow indicates the period when we switched from a constant applied force to a sinusoidal applied force in the x direction. To make it possible, we added a constant offset voltage and the output of a wave generator to the QPD signal input to the Pstage. This way, we obtained a reference point starting from 75 nm in the x direction and then oscillating between 50 and 100 nm (corresponding to an oscillating force between 0.1

#152555 - $15.00 USD Received 8 Aug 2011; revised 10 Sep 2011; accepted 10 Sep 2011; published 24 Oct 2011

and 0.5 pN, well inside the linear region of the trap), when we enabled the output of the wave generator (black trace in Fig. 5c).

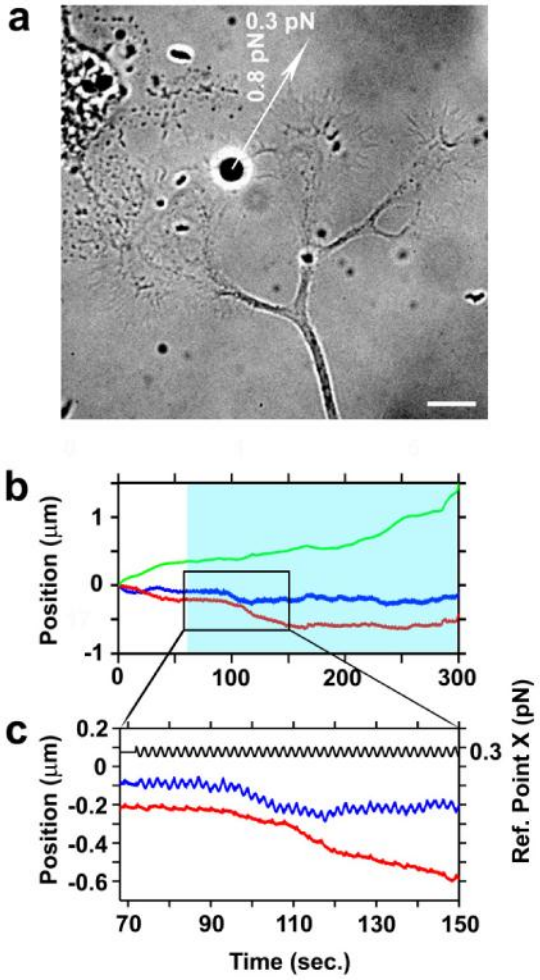

Fig. 5. Growth cones motility under time modulated tension. (a) Two contacting growth cones of a differentiating rat hippocampal neuron (7 DIV) with an attached poly-D-lysine coated bead. The white arrow indicates the constant force applied on the trapped bead. (b) Traces of the x, y, z coordinates of the tracked bead (in blue, red and green, respectively). Axes origin is at the left upper corner of the field of view in a. Traces are sampled at 2 KHz ($k_{x,y}$ = 4 fN/nm, k_z = 2 fN/nm). The blue shadow indicates when the applied force in the x direction is time modulated. Power at the sample, 3.8 mW. Bars, 8 μm. (c) Inset of the traces showed in b. The black line represent the tracked reference point in the x direction indicated in pN on the left side of the plot (oscillating frequency 0.3 Hz).

In Fig. 5c it is evident how such an offset affected only the blue trace (corresponding to the x bead coordinate), and how the tracking system still followed the bead displacement produced by the interacting growth cones. This type of experiments completed the range of available conditions to study the growth cone dynamics. We can compare the dynamics of a freely moving neurite tip with that of a growth cone under constant and prolonged applied tension, or under a dynamic force at distinct frequencies, to dissect the role of mechanical stimuli in growth cone navigation.

#152555 - $15.00 USD Received 8 Aug 2011; revised 10 Sep 2011; accepted 10 Sep 2011; published 24 Oct 2011

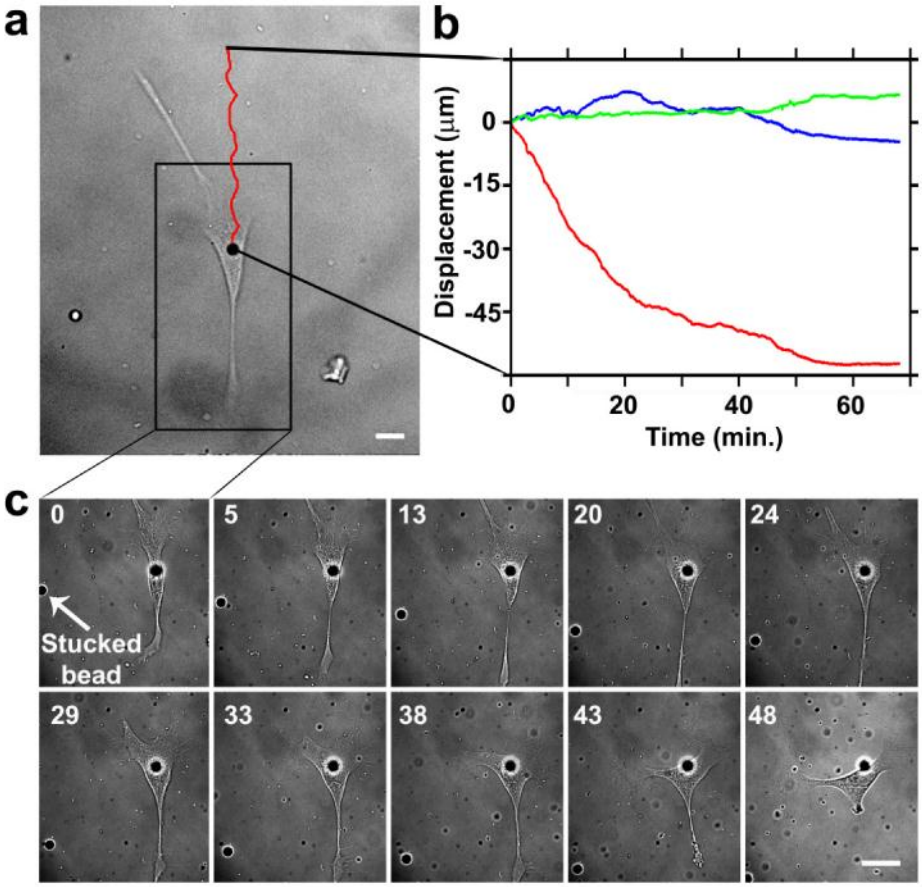

Fig. 6. Tracking a migrating adult dentate neural precursor cell. (a) An adult dentate neural precursor cell with a poly-D-lysine coated bead attached. The red line indicates the trace followed by the cell tracked by the attached bead. (b) Tiles of the cell motion during the interferometric tracking, acquired by bright-field imaging at 0.3 Hz. Numbers indicate minutes. (c) Traces of the x, y, z coordinates of the tracked bead (in blue, red and green, respectively). Axes origin is at the left upper corner of the field of view in a. Traces are sampled at 2 KHz ($k_{x,y}$ = 4 fN/nm, k_z = 2 fN/nm). Power at the sample, 3.8 mW. Bars, 8 μm.

In the last experiment reported in Fig. 6, we attached a bead to an adult dentate neural precursor cell (ADNPC) (2DIV), since we wanted to test our system on a fast migrating cell model (Fig. 6a). Figure 6a shows the migrating cell with the attached bead and the red trace indicate the entire recorded trajectory. Figure 6b illustrates how the cell changed morphology during motion, and in Fig. 6c it is shown the tracking of the cell for more than one hour over a distance exceeding the coarse range of the Pstage.

In conclusion, we could apply long-range interferometric tracking on living neuronal models, starting from the migrating progenitor cells, so as to arrive at the early phases of network development when neuritis of differentiating neurons establish their first connections.

4. Discussion

The physical and chemical composition of the substrate significantly modulates the visco-elastic properties of the cells. In case of a neuron, when axons are tightly bound to the extracellular matrix, less stretching occurs along the axon when mechanical tension is applied. The growth cone at the tip of a neurite produces forces causing low-speed transport

#152555 - $15.00 USD Received 8 Aug 2011; revised 10 Sep 2011; accepted 10 Sep 2011; published 24 Oct 2011

and stretching of the distal part of the axon, which ultimately creates neurite elongation [43]. During growth cone motility, the cell drives extracellular matrix remodelling, and vice versa the properties of the matrix itself regulate cell migration [44]. Periodic cycles of retraction and extension of lamellipodia showed to be correlated with formation of cell-matrix or cell-cell adhesion contacts [45]. The role of such intermittent interactions of the cell with the surrounding enviroment was explained as a mechanism used by the cell to test physical properties of the matrix, or to recruit molecular motors reinforcing the cellular adhesion contacts [46]. While static forces applied to a cell modulate the morphology and biophysical properties of the cell, i.e. laminar shear in vessels or tension between bone and muscles, cyclic tensions upregulate the assembly of focal adhesions [47]. In vitro studies already showed that the cell stiffness is correlated to the substrate rigidity and, in addition, that cells tends to migrate towards stiffer regions of the substrate due to a more efficient recruitment of molecular motors [48], until an equilibrium between the stiffness of the cell and the support is generated. The same is true for cell-cell interconnections, where a physiological tension has to be reached to make the connections stable and functional [49].

Optical tweezers represent a quantitative tool to apply biologically relevant forces to a living cell [14]. Up to now, optical tweezers studies on single cells have been applied over short periods of time or in a limited spatial range. In the present work, we have proposed a method to use very soft optical stiffness on differentiating cells for more than one hour on a spatial range limited only by the entity of the cell motion. The application of a constant force for a long period of time at the tip of a navigating neurite allowed us to observe how mechanical stretch can influence the growth velocity and direction. In case of applied compression, we could emulate the matrix rigidity the cell encounters during migration *in vivo*, with pN resolution [50]. Otherwise, the application of a dynamic load allowed us to simulate, by the bead, an approaching cell producing cyclic protrusions and retractions, and to observe how a neuron rearranges to create connections.

The high spatial and temporal resolution of the presented interferometric tracking system provides the possibility to capture the molecular details of the cellular dynamics [34]. This ability was exploited for the study of short (in time) and restricted (in space) biological phenomena, such as the connection of a growth cone to a neurite, illustrating the possibility to follow the dynamics of contact formation with a sensitivity not offered by other optical techniques. More interestingly, thanks to the proposed control system, the same resolution was also achieved for large cellular shifts, as in the case of a neuronal progenitor, allowing to detect the reshaping of the cell during its mesenchymal motion.

With the proposed architecture, we are able to track the cellular system with a low optical stiffness (a few femto-Newton per nanometer), obtaining in a high force clamp sensitivity with a low average power delivered at the sample (from 3.8 mW to a maximum of 5.5mW). This allows long-term measurements on cells with minimum photo-damage. Moreover, we show the possibility to modulate in time the force-clamp condition, by simply adding an arbitrary waveform as a set point to the detection system, to perform interferometric tracking of subcellular compartments under dynamic mechanical load [51]. In conclusion, the presented optical tweezers setup opens the possibility to observe single molecule events during relevant cellular phenomena with an unprecedent experimental flexibility.

Acknowledgment

We thank A. Parodi for his support during software development, and F. Succol and M. Nanni for their assistance in cell culture preparation. Special thanks to A. Blau for insightful discussion and suggestions, and to F. Spanò for critical reading of the text. This work was supported by grants from Telethon-Italy (GGP09134 to F. B.).

#152555 - $15.00 USD Received 8 Aug 2011; revised 10 Sep 2011; accepted 10 Sep 2011; published 24 Oct 2011